Langmuir

ARTICLE

pubs.acs.org/Langmuir

Automated Single-Molecule Imaging To Track DNA Shape

Juan Guan,[†] Bo Wang,[†] and Steve Granick*[,†,‡,§]

[†]Department of Materials Science and Engineering, [‡]Department of Chemistry, and [§]Department of Physics, University of Illinois, Urbana, Illinois 61801, United States

ABSTRACT: We describe a straightforward, automated line tracking method to visualize linear macromolecules as they rearrange shape by Brownian diffusion and under external fields such as electrophoresis. The analysis, implemented here with 30 ms time resolution, identifies contour lines from one end of the molecule to the other without attention to structure smaller than the optical resolution. There are three sequential stages of analysis: first, "feature finding" to discriminate signal from noise; second, "line tracking" to approximate those shapes as lines; and third, "temporal consistency check" to discriminate reasonable from unreasonable fitted conformations in the time domain. Automation makes it straightforward to accumulate vast quantities of data while excluding the unreliable parts of it. We implement this analysis on fluorescence images of λ-DNA molecules in agarose gel to demonstrate its capability to produce large data sets for subsequent statistical analysis.

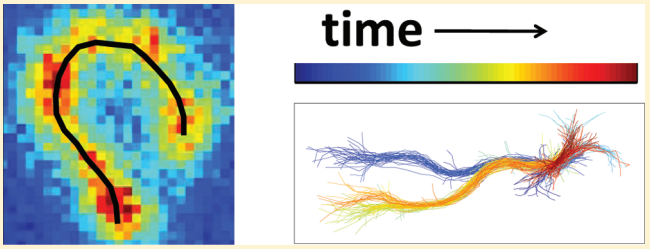

INTRODUCTION

This Article focuses on methods of image analysis that enable one to go beyond tracking the position of single molecules, to also analyze their internal conformations, in instances when molecules display shape fluctuations under various conditions ranging from thermal equilibrium to deformation under mechanical stress or other external field. As these changes are rapid, we are interested in real-time measurements during which the need to acquire data rapidly without signal averaging introduces experimental uncertainty. These problems of tracking internal degrees of freedom, which become technically feasible when the size of macromolecules exceeds the resolution of a microscope in one or more directions, apply especially to tracking biological macromolecules, among them filaments such as actin[1,2] and more flexible molecules such as DNA.[3−11]

Methods of image analysis could not be applied until recently to problems of this kind; indeed, in the early days the data were typically acquired by video microscopy, as for example in measurements of DNA and actin using fluorescence microscopy.[1−12] Almost from the beginning, special attention was given to direct observation of polymer conformations perturbed from equilibrium by mechanical force or electric field, but quantification was held back in part by the limited resolution of video cameras, in part by the inability of routinely analyze images using methods that would require significant computing power and data storage capacity. It is understandable that quantification to date has concerned largely radius of gyration and coarse measurement of shape anisotropy by measures such as the long axis and short axis components of fluorescence images in two-dimensional projection in the plane of a microscope.[13,14]

In addition, many of the early studies suffer from few statistics and involve analyzing a small number of images.[4,11,12] Yet from the beginning of this line of research, it was evident[4−10] that single-molecule analysis of chain conformations holds the promise to measure the distribution of chain conformations whose averages enter into important ensemble-averaged quantities, such as rheology and electrophoretic mobility. Nowadays, it is feasible to use inexpensive personal computers to facilitate analysis of polymer conformations with large statistics and high accuracy. This study is in the spirit of an earlier pioneering automated line tracking method, introduced to analyze actin,[15] which works well to analyze filamentous macromolecules that are stiff. The image analysis methods described below are designed to apply equally to more flexible macromolecules such as DNA.

The plan of this Article is to dwell primarily on the methods of automated image analysis we have developed to deal with this problem and to explain the logic that prompted the choice of those methods rather than others. These methods consist of three elementary stages: first, to discriminate the shapes of macromolecules from noise, which we refer to as "feature finding"; second, to approximate those shapes as lines, which we refer to as "line tracking"; and third, to discriminate reasonable from unreasonable fitted conformations in the time domain, which we refer to as "temporal consistency check". Finally, this Article presents two examples of applying the method. Although the methods are general and should readily be adaptable to other visualization techniques, here we illustrate the arguments using sample images from DNA in a fluorescent microscope. We focus on DNA that is driven by electric fields to adopt relatively extended conformations and a variety of shapes.

These methods, which build upon image processing methods reported earlier from this laboratory that at that time did not

Received: February 1, 2011
Revised: April 5, 2011
Published: April 21, 2011

consider internal degrees of freedom in the tracking of single molecules,[16,17] amount to approximating the true shape of linear macromolecules by renormalized curved lines, lines that are optimized to describe the shape within the limits of optical resolution.

The method is intrinsically coarse-grained, incapable of discriminating internal conformations smaller than the optical resolution, and hence yields lines designed to describe the contour of the macromolecule without attention to any structure smaller than the optical resolution. In the examples of the method presented below, this resolution was ~0.3 μm. As methods of super-resolution imaging[18] gain more widespread use, one can expect even more need for image analysis methods to analyze internal chain conformations at even higher resolution.

EXPERIMENTAL METHODS

The image analysis presented below was performed on data acquired in the following manner.

Fluorescence Microscopy. Data were acquired in epifluorescence mode, typically at a frame rate of 33 fps. A 532 nm excitation laser was focused at the rear focal point of an oil immersion objective (Zeiss, α-Plan Fluor 100×, NA = 1.45) with 2.5× postmagnification to image with a resolution of 64 nm × 64 nm per pixel. Fluorescence images were collected through the same objective and detected by a back-illuminated electron multiplying charge-coupled device (EMCCD) camera (Andor iXon DV-897 BV) after filtering out light from the excitation laser. The movies were converted into digital format and analyzed. A typical data set consists of 30 movies, each of them consisting of 4000 frames per movie acquired at 33 fps. The resulting data set of conformations typically amounts to $>10^4$ from thousands of molecules.

DNA Samples. Lambda-DNA (48.5 kbp, Promega) was labeled by covalently attaching dye, a RhB derivative (Mirus), to heteroatoms on DNA, at a labeling density of roughly one dye per 5 base pairs. Single-molecule measurements of DNA chain conformations were made in a miniature gel electrophoresis setup using agarose gel (final concentration 1.5% (w/v)), in 0.5× TBE buffer (45 mM Tris, 45 mM borate, 1 mM EDTA), the DNA being at picomolar concentration. Antiphotobleaching agent, ascorbic acid (SigmaAldrich), was present at a final concentration of 10 mM. A DC voltage was applied across two Pt electrodes to generate an electric field ranging from 6 to 16 V/cm.

METHODS OF IMAGE ANALYSIS

The purpose here is to quantify, within the limits of optical resolution, the linear shapes of CCD images that are noisy, faint, and diffraction-blurred. In the methods described below, we take the approach that it is better to reject data from consideration than to improperly include it in subsequent analysis. Therefore, especially in the third step of analysis consisting of checks of data consistency in the time domain, we reject up to 50% of the data acquisition frames. Examples of the variety of raw data are given in Figure 1c−e.

We begin by summarizing the algorithm:

(1) Filter digitized images to remove shot noise by performing a two-dimensional Gaussian smoothening.
(2) Calculate the mean and variance of the intensity of pixels in each image and keep high intensity pixels as candidate molecules.
(3) Group pixels/points into separate molecules using a specified threshold distance.
(4) Identify a longest path through each group of points using an intensity-weighted minimum spanning tree.

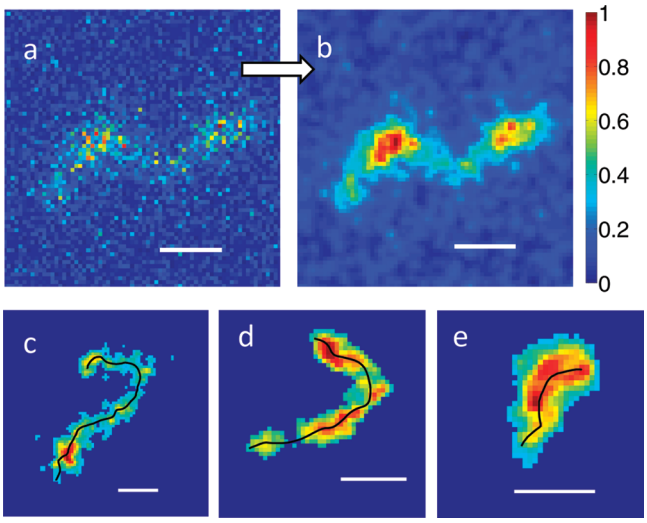

Figure 1. Examples of raw data in which λ-DNA (contour length 16 μm) displays various conformations in an optical microscope. Color bar corresponds to relative intensity within each image. (a) A typical unprocessed image as input raw data. (b) A local Gaussian filter reduces noise significantly. (c−e) Additional examples of various polymer conformations with final line tracking results (black line) overlaid. Scale bar: 1 μm.

(5) Local quadratic fits to adjust the positions of the pixels.
(6) Additional position refinement by Gaussian fit to find the center using the cross-section intensity profile at each position.
(7) Find a new longest path from these points by generating a new minimum spanning tree from these points.
(8) Smooth the line with a discrete wavelet filter.
(9) Perform prescreening to reject unreasonable lines such as those which drastically fluctuate in length, are looped, or are from molecules that are out of focus.
(10) Compare line with previous and subsequent lines in time. If two lines are similar from a set of around 20 frames, then they may be retained for analysis.

Identifying Each DNA Molecule. For various practical reasons, despite one's most careful efforts to optimize image quality, the signal-to-noise ratio is never satisfactory in unprocessed images (Figure 1a). First, the finite DNA concentration results in background fluorescence from other molecules that contribute to the image despite being located outside the focal plane. Second, the DNA that we track moves rapidly under electrophoresis, leaving limited time to collect photons at each position. Third, the elongation of chains under electric field lessens the local fluorophore density. We find that applying a Gaussian filter with a width of 1 pixel locally at each pixel, with Gaussian weighted contribution of intensity from neighboring pixels, significantly reduces noise without compromising the main features of a DNA molecule (Figure 1b).

As each image consists primarily of background, only a few pixels representing the dilute DNA molecules of interest, we estimate background intensity noise from the mean intensity at each pixel, and we estimate noise level from the variance of these pixel intensities. After subtracting this background from each pixel in the image, we retain for subsequent analysis only pixels at which the residual intensity exceeds a threshold, typically set to be 7−10 times the noise level. Control checks show that

dx.doi.org/10.1021/la200433r |Langmuir 2011, 27, 6149–6154

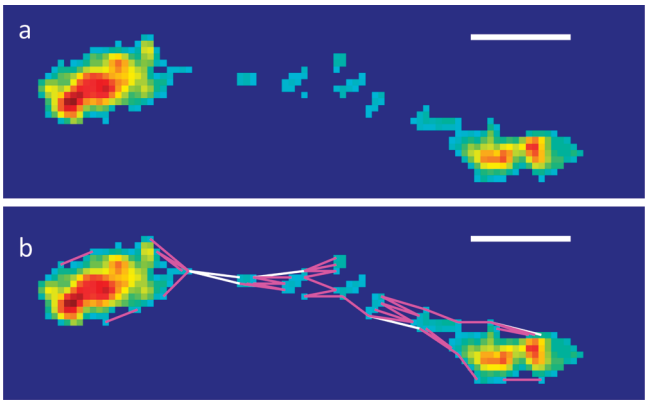

Figure 2. Feature finding: Grouping pixels into one DNA molecule or several according to the threshold distance between pixels. (a) An example of an image in which only a fraction of the middle pixels have high enough intensity to be recognized as signals. (b) The connections between pixels discriminate whether they cluster into one grouping or several. The leftmost two white connections are critical; if not present, this image is treated as two groupings, each one from a different molecule. The pink connections are separated by 5−8 pixels. The white connections are separated by 8−9 pixels. Scale bar: 1 μm. Color bar is the same as in Figure 1.

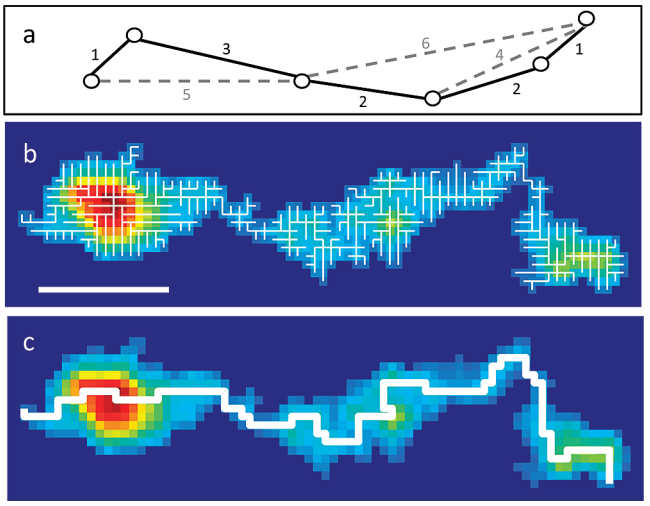

Figure 3. Line tracking: Using minimum spanning tree analysis to find a longest path through pixels to identify a line through the DNA molecule. (a) Schematic illustration of the notion of minimum spanning tree. The edges belonging to the minimum spanning tree are drawn in solid lines, whereas other edges are drawn with dashed lines. Next to each edge, the indicated numbers specify the relative weight. (b) Example of an intensity-weighted minimum spanning tree (white) overlaid onto real data. (c) For the data in panel (b), a longest path (thick white line) is identified from analyzing the minimum spanning tree. Scale bar: 1 μm.

subsequent line tracking does not depend sensitively on the detailed choice of threshold value, nor on whether the image of the DNA is included in estimation of the background.

Next, the image analysis makes judgments to decide whether two features close in space belong to a single molecule. It is a problematical question because low signal-to-noise ratio pixels may in principle register the absence of DNA, but also may indicate that low intensity parts of the molecule, in some cases even vanishingly low intensity due to various reasons discussed earlier in this section. Figure 2a illustrates a stretched DNA whose middle part presented intensity less than an intensity threshold. To analyze this situation, first we connect pixels whose distance is less than a threshold and consider tentatively the connected pixels to come from a single molecule. Depending on the threshold selected, the pixels in an image then cluster into either a single grouping or several. For example, using a threshold distance of 8 pixels, Figure 2b presents two clusters of pixels, whereas a threshold of 9 pixels implies just a single cluster of pixels; the difference depends on whether critical connections are allowed or disallowed by that threshold (white lines in Figure 2b). To automate the process of line tracking, to perform this grouping of pixels first we apply a fixed threshold and analyze the best line through the implied grouping. Unreasonable lines are then removed at a later stage of analysis through the automated temporal consistency checks discussed in a later section.

Tracing a Line through Each DNA Molecule. This relies on the concept of a minimum spanning tree, a concept in graph theory that quantifies the shortest path length between nodes in an image.[19] Here, the nodes in the image are the pixels of the molecule defined from the previous section. Figure 3a illustrates the concept schematically, and Figure 3b illustrates it for a given set of data acquired in our experiments. First, a tree is constructed by connecting every two pixels. However, because some pixels are bright and others are dim, and we wish to preferentially include pixels of high intensity to minimize the chance of resulting lines being trapped on noise pixels, the connection length between pixels is assigned not simply as the spatial distance by which they are separated, but weighted by the inverse of their sum intensity. A minimum spanning tree is then generated choosing from existing connections based on each connection length. We find that this feature of intensity weighing is often necessary but that the exact intensity weighing method is not critical in line tracking; for example, an alternative weighting, exponential weighting according to intensity, gives similar results. Searching through this minimum spanning tree, one can find one path between two termini that contains the largest number of pixels: this is the longest path through this molecule (Figure 3c).

To yield the final line tracking result (Figure 4a), we follow a four-step progressive refinement of the result. First, to the line, we perform a polynomial fit, typically a quadratic fit, locally on adjacent pixels (Figure 4b). The local fit is preferable to fitting the entire line with a polynomial because the overall shape is sometimes highly curved. An additional advantage of local fitting is that to improve accuracy, one can select at each point which coordinate, horizontal x or vertical y, to fix or fit. The choice to fix or fit is done by performing both x and y fits and choosing automatically whichever minimizes local fitting error. After this automated process, each pixel is reassigned a new point that has a modified x or y position. This local fitting with flexible x or y is most faithful to the original shape than a single global polynomial fit and sometimes the only possible way to fit a highly curved shape.

To further smooth the line, the second step is to fit the cross-section intensity profile at each point along it to a Gaussian intensity profile, the principle being that diffraction-limited images are expected to be described by this function. The position of each pixel along the line is then accordingly adjusted to the center of the Gaussian (Figure 4c); typically, this adjustment is on the order of one pixel. In this fitting, the orientation of the cross section is taken to be perpendicular to the tangent line at each point. As the coordinates at this stage of the analysis are typically

dx.doi.org/10.1021/la200433r |*Langmuir* 2011, 27, 6149–6154

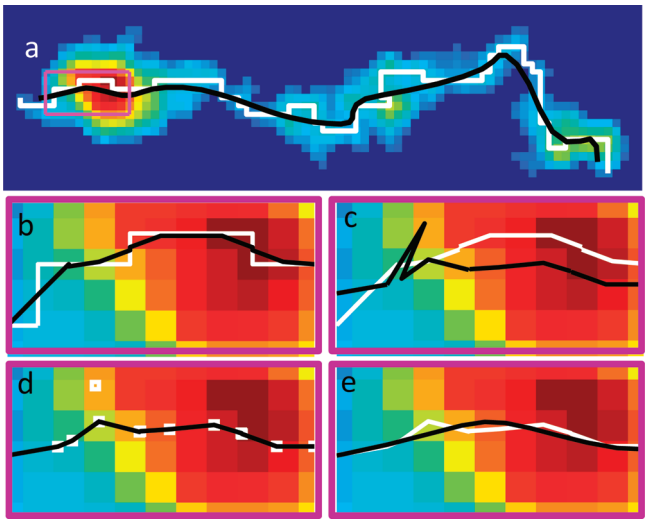

Figure 4. Four-step refinement of the line identified in each single image. The highlighted region in panel a, magnified in panels b−e, is used to illustrate how a line changes from each step to the next step during the refinement procedure. In panels b−e, starting lines and symbols are white, and the line resulting from that step is drawn in black. (a) Starting from a longest path connecting pixels (white, same as in Figure 3c), a four-step refinement yields the final line tracking result (black). (b) A polynomial fit. (c) A Gaussian fit to recenter. (d) A minimum spanning tree through the resulting points in (c). (e) Wavelet smoothening. See text for details.

not located on integer pixel positions, the intensity at each point is calculated on the basis of the surrounding four pixels (integer coordinates) via linear interpolation.

Third, the minimum spanning tree is recalculated from the points that resulted from the second step (Figure 4d). The process to do so is the same as before, except that adjacent points are linked without intensity weighing. This step is to deal with occasional failures in the second step to find an accurate tangent direction and hence the correct cross section. For example, the radical jag in Figure 4c came from this occasional failure. Although the line looks jagged in this zoom-in presentation, this new position deviates less than two pixels from the original. We exclude these anomalous positions nonetheless using a minimum spanning tree.

Last, high-frequency noise is removed using a wavelet filter (Figure 4e). It is convenient to employ a discrete wavelet transform based on the Daubechies-16 wavelet of the line. The level 2 coefficients, which are the decomposition in high frequency range corresponding to 2−4 neighboring points, are soft thresholded such that coefficients exceeding the threshold, δ, in magnitude were pushed toward zero by δ, while those less than or equal to δ were set to zero. The threshold is calculated through the universal threshold, $\delta = \tilde{\sigma}(2 \ln N)^{1/2}$, where N is total number of points and $\tilde{\sigma}$ is estimated via median absolute deviation (MAD) of coefficients, $\tilde{\sigma} \equiv (\text{median}\{|c_i^{x,y}{}_{=1,\ldots,N}(2)|\})/0.6745$. The choice of coefficients, working at the level corresponding to 2−4 neighboring points, is primarily to remove high frequency noise in the line. The smoothened line is obtained by inverse transforming the coefficients after thresholding.

Temporal Consistency Checks. The idea is to err on the side of caution: we aim to exclude questionable data from the data set that we construct for subsequent analysis. As the automated nature of this data analysis makes it straightforward to accumulate vast

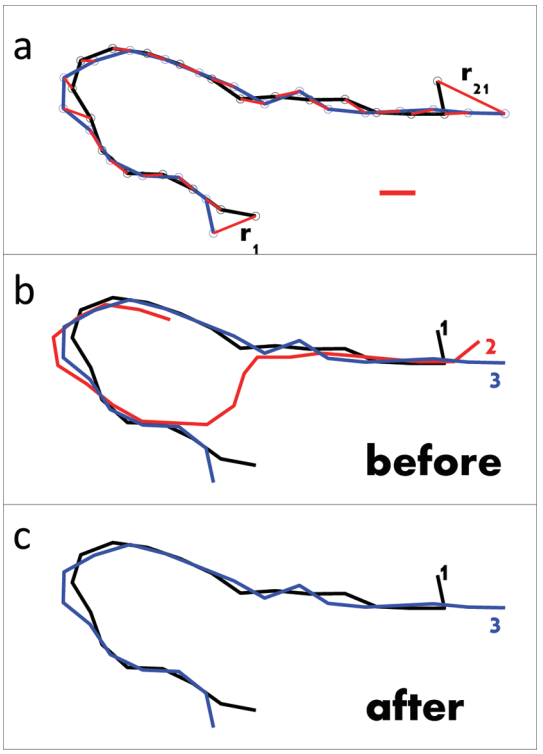

Figure 5. Tests of temporal consistency: Selecting reasonable lines from temporal comparison of images at different times. (a) Each line is overlaid with 21 notional fiducial points. Within the temporal vicinity of a few seconds, the average distance between each point on any two lines is evaluated (red lines). When this is less than a threshold designation of similarity, the lines are deemed valid and kept. Lines that fail this similarity criterion are rejected as physically unreasonable. In this typical example, the threshold is 0.4 μm. (b) Raw data: Three lines from the level of analysis in Figure 4. (c) Outcome of the test for temporal consistency: Line 2 is rejected. The text describes additional prescreenings included in these checks. Scale bar is 0.4 μm.

quantities of data, there is no disadvantage to excluding from analysis the unreliable parts of it.

As a premise, we take the view that when image acquisition is rapid relative to those conformational fluctuations of DNA that occur on distances resolvable within optical resolution, a true line is likely to be similar to those close to it in time, but an unreasonable line is unlikely to satisfy this criterion. Dissimilar lines may arise for a number of uninteresting reasons: mistaken grouping of data in the first level of analysis to identify the starting DNA molecule; molecules whose extension is so limited that it hardly exceeds the optical resolution; molecules out of focus; and an error in generating the minimum spanning tree. Reasoning from this premise, we compare each line, acquired at a given moment in time, to its antecedents and progeny over the span of a few seconds. When two lines are similar, both are regarded valid and included in the final set of lines.

To implement this idea, the line that traces the contour of each DNA molecule is divided into 21 notional fiducial markers of equal spacing along the line and the average distance by which a line is displaced from another line within the temporal vicinity of a few seconds is measured against a threshold value, as drawn schematically in Figure 5a. A small average distance means two lines are similar and are likely to both be valid. After this selection, anomalous lines are removed, as illustrated in Figure 5b and c.

dx.doi.org/10.1021/la200433r |*Langmuir* 2011, 27, 6149–6154

For the experimental tests reported below, we find selected lines and subsequent analysis results converge in a wide threshold window between 0.4 and 0.8 μm, but it is likely that the optimal threshold will depend on the application to which this method is put. We typically choose a threshold value of 0.4 μm to insist on high accuracy. It is our experience that a more stringent threshold sometimes fails to capture the dynamics in conformation change and might introduce bias in the data set.

We find that precision of the final set of lines is improved by performing a series of prescreenings before the selection. This automated process searches for many anomalous features; when any of them is identified, that frame of the data set is excluded from analysis. First, we remove regions where line length fluctuation with time is frequent and unreasonably drastic. We compare the fluctuation before and after applying a third-order Savitzky–Golay FIR smoothing filter. Frames associated with large discrepancy (>1.3 μm) are excluded. Second, lines that are too short relative to their neighbors in time are considered to be the likely result of partial features due to incorrect grouping of molecules or else to low intensity parts not identified as signal; as these anomalously short lines can potentially introduce large errors in further quantitative analysis, they are removed. Typically we reject, as unreasonable, putative data whose length is shorter by 1 μm than in adjacent frames. In the experimental system that we study, we find the most rapid length fluctuations to occur about 1 order of magnitude slower than the criterion we use here to reject potentially wrong data. Third, we exclude dim molecules that have both low shape anisotropy and large short axis component as they are likely to be out of focus. Fourth, the size of a candidate molecule is used to further exclude partial features. Fifth, the end-to-end distance of a line is considered, relative to the length of that line; if the ends appear to loop together too closely, as can happen when the image area is close to the optical diffraction limit even though it is less than one-half the mean radius of gyration of the system we study here, this also is considered likely to be anomalous and is excluded from further analysis.

It is true that, in principle, the exclusion of data might risk biasing the data set. Checking the radius of gyration before and after this selection, we find no bias toward a subpopulation of molecules. The distribution of radius of gyration remains unchanged indicating that the criteria, by which lines are considered to be unreasonable, do not depend on size of the molecule. The exception is that the smallest 10% of molecules (radius of gyration smaller than the diffraction limit, which corresponds to less than one-half the mean radius of gyration of λ-DNA) do not contribute to the final set of lines. Line tracking should not be expected to work well in this situation. In addition, features so small are likely to be either noise or fragmented molecules, and in this respect it is proper to exclude them. Testing directly for hypothetical bias of the data, we also measured average DNA velocity along the electric field direction, with and without the selection of data just described, and found no meaningful difference.

APPLICATION TO SPECIFIC SYSTEMS

To illustrate how automated line tracking allows visualization of polymer conformation changes in dynamic processes, we now present two examples, both of which will be fully explored in subsequent reports from this laboratory. The point of these examples is simply to illustrate the quality of data that can be obtained routinely, with large statistics and high fidelity, using the image analysis methods presented in this Article.

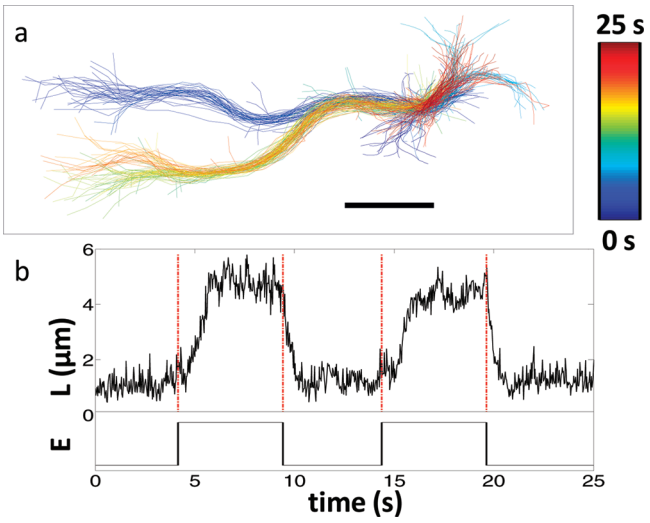

Figure 6. An example of applying automated line tracking analysis. A λ-DNA molecule with one end attached to the agarose gel in which it is embedded is subjected to repeated stretch and release using a square wave electric field alternating with period about 10 s between 16 and 0 V/cm. (a) Overlay of all lines tracked over the time of 25 s, at 33 frames per second, showing the distribution of paths by which the molecule threads through the gel. Color bar denotes time. Scale bar: 1 μm. (b) Lower panel: Square-wave electric field applied to the DNA over 25 s. Upper panel: Length fluctuation of lines tracked during this time window, showing stretch and retraction. Vertical dashed lines show the time at which the electric field switches on and off.

Figure 6 illustrates experiments in which a λ-DNA molecule, attached at one end to the agarose gel in which it is embedded, is subjected to repetitive stretch and release by applying a periodic electric field. In Figure 6a, which overlays lines tracked from hundreds of frames when this molecule was subjected to repeated stretching and releasing from a square wave, one notices that stretch–retraction events differ subtly from one another, differing not just in times for these processes to be accomplished, but also in the paths by which the molecule is threaded through the gel. Figure 6b illustrates a small number of the accompanying length fluctuations during these stretch and release events. Whereas stretching and recoiling both transpire on the time scale of 1 s, a recoil process is also clearly evident between two stretches, before the molecule takes on a different path.

Figure 7 illustrates data from a different experiment: λ-DNA migrating through agarose gel under a DC field of 16 V/cm. This set of data, consisting of $\sim 4 \times 10^4$ evaluations of the curvilinear end-to-end distance of the molecule, shows clearly the statistical nature of the curvilinear end-to-end distance: while the mean value is well-defined, and the most probable value is well-defined, the distribution around averages is large.

PROSPECTS

In this computer age, with large computing power and digital storage capacity readily accessible, one can use inexpensive personal computers to facilitate image analysis of optical images. Here, we have introduced automated line tracking methods applicable to tracing the linear coarse-grained shapes of biomolecules, those shapes larger than the optical diffraction limit, and have illustrated their application to analyzing the conformations of fluorescent-labeled λ-DNA when it is stretched by electric

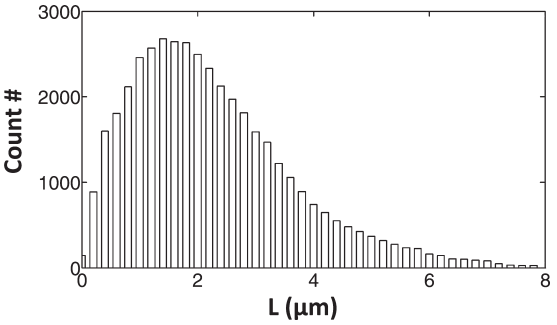

Figure 7. A second example of applying automated line tracking analysis. This figure shows a histogram of curvilinear end-to-end distance defined by line tracking, as λ-DNA migrates through agarose gel under a DC electric field of 16 V/cm. The data set was 30 movies, each of them consisting of 4000 frames per movie acquired at 33 fps. Number of observations is plotted against length with bin size 0.2 μm.

fields. These automated methods enable the facile acquisition of large data sets and by rational extension should readily be adaptable to analysis of data obtained from other visualization methods. It is different in spirit from principal component analysis of DNA, which expresses dynamic information in a virtual phase space of orthogonal basis sets that can be problematical to interpret physically.[20]

While the fidelity of tracking reported here is believed to have been optimized within the limits achievable using optical resolution, it is certainly the case that this image analysis is limited in resolution. The line tracking introduced in this study represents a coarse-grained representation of the actual contour of λ-DNA; this is why, for example, even the longest lengths plotted in Figure 7 are a factor of 3 smaller than the known contour length of the molecule, 16 μm. Thus, while these methods are well adapted for quantifying time scales of dynamic processes (illustrated in Figure 6) and also their distributions (illustrated in Figure 7), the numerical values of the lines do not, at the present time, have one-to-one correspondence with the actual molecular makeup, but should be viewed instead as coarse-grained representations. We remark that this coarse-graining can carry physical meanings overlapping with the classic bead−spring notation, especially when the optical resolution limit coincides with the fundamental length scale of the system; for example, the pore size of agarose gel, ~200 nm, nearly coincides with the diffraction limit in this study. Provocatively, the same also holds for many other biomacromolecular solutions.

AUTHOR INFORMATION

Corresponding Author

*E-mail: sgranick@uiuc.edu.

ACKNOWLEDGMENT

We thank Kejia Chen for discussions. This work was supported by the U.S. Department of Energy, Division of Materials Science, under Award No. DEFG02-02ER46019. For instrumentation, we acknowledge support from NSF-CBET-0853737.

REFERENCES

(1) Kas, J.; Strey, H.; Sackmann, E. *Nature* **1994**, *368*, 226.
(2) Wang, B.; Guan, J.; Anthony, S. M.; Bae, S. C.; Schweizer, K. S.; Granick, S. *Phys. Rev. Lett.* **2010**, *104*, 118301.
(3) Perkins, T. T.; Smith, D. E.; Chu, S. *Science* **1994**, *264*, 819.
(4) Perkins, T. T.; Quake, S. R.; Smith, D. E.; Chu, S. *Science* **1994**, *264*, 822.
(5) Perkins, T. T.; Smith, D. E.; Larson, R. G.; Chu, S. *Science* **1994**, *268*, 83.
(6) Quake, S. R.; Babcock, H. P.; Chu, S. *Nature* **1997**, *388*, 151.
(7) Perkins, T. T.; Smith, D. E.; Chu, S. *Science* **1997**, *276*, 2016.
(8) Smith, D. E.; Chu, S. *Science* **1998**, *281*, 1335.
(9) Smith, D. E.; Babcock, H. P.; Chu, S. *Science* **1999**, *283*, 1724.
(10) Schroeder, C. M.; Babcock, H. P.; Shaqfeh, E. S. G.; Chu, S. *Science* **2003**, *301*, 1515.
(11) Howard, T. D.; Holzwarth, G. *Biophys. J.* **1992**, *63*, 1487.
(12) Gurrieri, S.; Rizzarelli, E.; Beach, D.; Bustamante, C. *Biochemistry* **1990**, *29*, 3396.
(13) Bonthuis, D. J.; Meyer, C.; Stein, D.; Dekker, C. *Phys. Rev. Lett.* **2008**, *101*, 108303.
(14) Hsieh, C.-C.; Balducci, A.; Doyle, P. S. *Macromolecules* **2007**, *40*, 5196.
(15) Brangwynne, C. P.; Koenderink, G. H.; Barry, E.; Dogic, Z.; MacKintosh, F. C.; Weitz, D. A. *Biophys. J.* **2007**, *93*, 346.
(16) Anthony, S. M.; Granick, S. *Langmuir* **2009**, *25*, 8152.
(17) Anthony, S. M.; Zhang, L.; Granick, S. *Langmuir* **2006**, *22*, 5266.
(18) Fernández-Suárez, M.; Ting, A. Y. *Nat. Rev. Mol. Cell Biol.* **2008**, *9*, 929.
(19) Cormen, T. H.; Leiserson, C. E.; Rivest, R. L.; Stein, C. *Introduction to Algorithms*, 2nd ed.; MIT Press and McGraw-Hill: New York, 2001.
(20) Cohen, A. E.; Moerner, W. E. *Proc. Natl. Acad. Sci. U.S.A.* **2007**, *104*, 12622.